

1 **Supplement of**

2 **Source Apportionment of Carbonaceous Aerosols in Beijing with Radiocarbon**
3 **and Organic Tracers: Insight into the Differences between Urban and Rural Sites**

4 **Siqi Hou et al.**

5 *Correspondence to:* Roy M. Harrison (r.m.harrison@bham.ac.uk), Zongbo Shi (z.shi@bham.ac.uk)

6

7 **Influence from Regional Transport**

8 During the wintertime, air masses transported to Beijing were mainly from Inner Mongolia, Shanxi
9 and Hebei, where the open burning activities were associated with maize straw (Zhang et al., 2019).
10 During summer, air masses from Shandong, Hebei, Liaoning and Tianjin may bring particles from
11 burning of wheat straw. However, for Inner Mongolia and Shanxi, little wheat is grown in these areas
12 (Zhang et al., 2019; Zhou et al., 2017) and the influence of wheat straw burning is less important. The
13 fire spot intensity, transport direction and sources of biomass burning are summarized in Table S1.

14 The high fire spot intensity indicates a strong likelihood of regional transport. However, the
15 concentrations of LG would decrease with atmospheric transport by aging, varying with
16 environmental conditions (Bhattarai et al., 2019), which can be used to infer the influence from
17 regional transport and local emissions. For example, with similar $PM_{2.5}$ concentrations, the LG
18 concentration on 26 November was much lower than that on 3 December. Considering the different
19 intensity of fire spots between the two days, LG on 26 November may arise more from regional
20 transport instead of local emissions. Moreover, the LG concentration on 2 December was similar to
21 that on 3 December, but the $PM_{2.5}$ concentration was much lower. This implies a contribution from
22 local sources in addition to regional transport on 2 December.

23 **Detailed Method of Ratio Selection and Sensitivity Test for Quantification of Biomass Burning**

24 As mentioned in the main text, softwood, maize straw and wheat straw are the main types of biomass
25 fuels used within the region. The ratios of EC/OC and OC/LG from softwood, maize straw and wheat
26 straw are summarized in Table S2.

27 As the fraction of LG from wood burning (f_{wood}) and straw burning ($f_{straw} = 1 - f_{wood}$) are each in the
28 range of 0 to 1, only those matching this limitation were selected when calculating OC_{bb} . Emission
29 factors of LG from various biofuels showed that the LG emission from wheat straw was hundreds of
30 times higher than from the values for wood combustion, while the emission factors are similar
31 between maize and wood (Yan et al., 2018). It means that although the consumption of wheat straw
32 may be less than that of wood, LG emission from wheat straw may exceed that from wood, and f_{wood}

may be quite small in summer. Besides, the sum of calculated OC_{straw} and OC_{wood} should not exceed the measured OC_{nf} concentrations, which is another limitation for selecting EC/OC and OC/LG ratios. Hence, ratios of softwood from No. 25 to No. 37 in Table S3 with ratios of maize (No. 48 in Table S3) were used for the wintertime, and No. 30-37 with No. 42-45, 50 from softwood and wheat straw respectively were used in the summertime estimation of f_{wood}

OC_{bb} from each type of softwood and crop straw combination can be estimated once f_{wood} was confirmed, and then these were averaged. To further assess the sensitivity of the calculated OC_{bb} results to the different ratio sets, concentrations of OC_{bb} for each set of ratios have been plotted vs. the averaged values (Fig. S4). Compared to OC_{wood} , concentrations of OC_{straw} show a small spread, and are in narrow ranges. It means the OC_{straw} are less affected by the varying ratios, as the range of ratios is smaller. According to Fig. S4, there are large uncertainties attached to the estimated values of OC_{wood} , but not OC_{straw} . The uncertainties from OC_{bb} can further affect the estimation of OC from cooking, but have no influence on estimates of SOC, which are determined from the $(OC/EC)_{\text{min}}$ ratios. The accuracy of this extended Gelencsér method would increase if the softwood types and ratios were confirmed.

The concentrations and contributions of OC_{bb} are shown in Fig. S5. The uncertainties of OC_{bb} are calculated considering the uncertainties of EC_{nf} and LG:

$$u(OC_{\text{bb}}) = \sqrt{\sum \left[\left(\frac{a-b}{ac-bd} \right)^2 u(EC_{\text{nf}})^2 + \left(\frac{abc-abd}{ac-bd} \right)^2 u(LG)^2 \right]}$$

where $a = (OC/LG)_{\text{wood}}$, $b = (OC/LG)_{\text{straw}}$, $c = (EC/OC)_{\text{wood}}$, and $d = (EC/OC)_{\text{straw}}$.

The average uncertainty of the LG concentration is 15%. The uncertainty of EC_{nf} is calculated by combining all the uncertainties from EC concentrations, f_{NF} , f_{M} and f_{ref} . The average uncertainty of OC_{bb} is 48.6%.

Determination of $OC/EC_{\text{f, min}}$ and $OC/EC_{\text{nf, min}}$ ratios and the estimation of POC_{f} and POC_{nf}

OC/EC ratios are seen as an indicator of aerosol emission sources to estimate the POC and SOC concentrations. ^{14}C analysis can provide OC to EC ratios from fossil and non-fossil sources ($\text{OC}/\text{EC}_\text{f}$ and $\text{OC}/\text{EC}_\text{nf}$). Herein, we use the lowest $\text{OC}/\text{EC}_\text{f}$ and $\text{OC}/\text{EC}_\text{nf}$ ratios ($\text{OC}/\text{EC}_\text{f, min}$ and $\text{OC}/\text{EC}_\text{nf, min}$, respectively) to represent primary OC/EC emission ratio to calculate primary fossil-derived and non-fossil-derived OC (POC_f and POC_nf) respectively. To avoid the overestimation of POC_f and POC_nf from the measured $\text{OC}/\text{EC}_\text{f, min}$ and $\text{OC}/\text{EC}_\text{nf, min}$ due to the limited samples for ^{14}C analysis in this study, it is necessary to evaluate $\text{OC}/\text{EC}_\text{nf, min}$ and $\text{OC}/\text{EC}_\text{f, min}$ ratios for the whole sampling period.

The relationship of $\text{OC}/\text{EC}_\text{nf}$ and $\text{OC}/\text{EC}_\text{f}$ with OC/EC can be described as follow,

$$\frac{\text{OC}}{\text{EC}_\text{nf}} = \frac{f_{\text{NF,OC}}}{f_{\text{NF,EC}}} \times \frac{\text{OC}}{\text{EC}}$$

$$\frac{\text{OC}}{\text{EC}_\text{f}} = \left(\frac{1-f_{\text{NF,OC}}}{1-f_{\text{NF,EC}}} \right) \times \frac{\text{OC}}{\text{EC}}$$

where $f_{\text{NF, OC}}$ and $f_{\text{NF, EC}}$ are the non-fossil fractions of OC and EC, $(1-f_{\text{NF, OC}})$ and $(1-f_{\text{NF, EC}})$ are the fossil fractions of OC and EC.

Ratios of $\text{OC}/\text{EC}_\text{nf}$ are determined by $\frac{f_{\text{NF,OC}}}{f_{\text{NF,EC}}}$ and OC/EC , therefore $\text{OC}/\text{EC}_\text{nf, min}$ can be roughly quantified by multiplying the lowest 5% OC/EC ratios with the lowest two $\frac{f_{\text{NF,OC}}}{f_{\text{NF,EC}}}$ ratios. Similarly, $\text{OC}/\text{EC}_\text{f, min}$ can be estimated by multiplying the lowest 5% OC/EC ratios with the lowest two $\left(\frac{1-f_{\text{NF,OC}}}{1-f_{\text{NF,EC}}} \right)$ ratios. The estimated $\text{OC}/\text{EC}_\text{nf, min}$ and $\text{OC}/\text{EC}_\text{f, min}$ ratios for IAP and PG sites in winter and summer sampling period were listed in Table S4. The estimated $\text{OC}/\text{EC}_\text{nf, min}$ and $\text{OC}/\text{EC}_\text{f, min}$ ratios are within the values of OC/EC emission ratios from coal combustion (1.5-15), traffic emission (0.69-1.01), and biomass burning (3-7) (Ni et al., 2018). Higher $\text{OC}/\text{EC}_\text{f, min}$ ratios in winter are consistent with the fact of elevated coal combustion compared to traffic emissions. It indicated the evaluation of $\text{OC}/\text{EC}_\text{nf, min}$ and $\text{OC}/\text{EC}_\text{f, min}$ ratios are reasonable.

77

78 **References**

- 79 Bhattarai, H., Saikawa, E., Wan, X., Zhu, H., Ram, K., Gao, S., Kang, S., Zhang, Q., Zhang, Y., Wu,
80 G., Wang, X., Kawamura, K., Fu, P., and Cong, Z.: Levoglucosan as a tracer of biomass burning:
81 Recent progress and perspectives, *Atmos. Res.*, 220, <https://doi.org/10.1016/j.atmosres.2019.01.004>
82 20-33, 2019.
- 83 Dhammapala, R., Claiborn, C., Jimenez, J., Corkill, J., Gullett, B., Simpson, C., and Paulsen, M.:
84 Emission factors of PAHs, methoxyphenols, levoglucosan, elemental carbon and organic carbon from
85 simulated wheat and Kentucky bluegrass stubble burns, *Atmos. Environ.*, 41, 2660-2669,
86 <https://doi.org/10.1016/j.atmosenv.2006.11.023>, 2007.
- 87 Fine, P. M., Cass, G. R., and Simoneit, B. R. T.: Chemical characterization of fine particle emissions
88 from fireplace combustion of woods grown in the northeastern United States, *Environ. Sci. Technol.*,
89 35, 2665-2675, <https://doi.org/10.1021/es001466k>, 2001.
- 90 Fine, P. M., Cass, G. R. and Simoneit, B. R. T.: Chemical characterization of fine particle emissions
91 from the fireplace combustion of woods grown in the southern United States, *Environ. Sci. Technol.*,
92 36, 1442-1451, <https://doi.org/10.1021/es0108988>, 2002.
- 93 Fine, P. M., Cass, G. R., and Simoneit, B. R. T.: Chemical characterization of fine particle emissions
94 from the wood stove combustion of prevalent United States tree species, *Environ. Eng. Sci.*, 21, 705-
95 721, <https://doi.org/10.1089/ees.2004.21.705>, 2004.
- 96 Fushimi, A., Saitoh, K., Hayashi, K., Ono, K., Fujitani, Y., Villalobos, A. M., Shelton, B. R., Takami,
97 A., Tanabe, K. & Schauer, J. J.: Chemical characterization and oxidative potential of particles
98 emitted from open burning of cereal straws and rice husk under flaming and smoldering conditions,
99 *Atmos. Environ.*, 163, 118-127, <https://doi.org/10.1016/j.atmosenv.2017.05.037>, 2017.
- 100 Gonçalves, C., Alves, C., Evtyugina, M., Mirante, F., Pio, C., Caseiro, A., Schmidl, C., Bauer, H.,
101 and Carvalho, F.: Characterisation of PM₁₀ emissions from woodstove combustion of common
102 woods grown in Portugal, *Atmos. Environ.*, 44, 4474-4480,
103 <https://doi.org/10.1016/j.atmosenv.2010.07.026>, 2010.
- 104 Hays, M. D., Geron, C. D., Linna, K. J., Smith, N. D., and Schauer, J. J.: Speciation of gas-phase
105 and fine particle emissions from burning of foliar fuels, *Environ. Sci. Technol.*, 36, 2281-2295,
106 <https://doi.org/10.1021/es0111683>, 2002.
- 107 Hays, M. D., Fine, P. M., Geron, C. D., Kleeman, M. J., and Gullett, B. K.: Open burning of
108 agricultural biomass: Physical and chemical properties of particle-phase emissions, *Atmos. Environ.*,
109 39, 6747-6764, <https://doi.org/10.1016/j.atmosenv.2005.07.072>, 2005.
- 110 Mazzoleni, L. R., Zielinska, B., and Moosmüller, H.: Emissions of levoglucosan, methoxy phenols,
111 and organic acids from prescribed burns, laboratory combustion of wildland fuels, and residential
112 wood combustion, *Environ. Sci. Technol.*, 41, 2115-2122, <https://doi.org/10.1021/es061702c>, 2007.

113 Ni, H. Y., Huang, R.-J., Cao, J. J., Liu, W. G., Zhang, T., Wang, M., Meijer, H. A. J., and Dusek, U.:
 114 Source apportionment of carbonaceous aerosols in Xi'an, China: insights from a full year of
 115 measurements of radiocarbon and the stable isotope ^{13}C , *Atmos. Chem. Phys.*, 18, 16363-16383,
 116 <https://doi.org/10.5194/acp-18-16363-2018>, 2018.

117 Sang-Arlt, X., Fu, H. X., Zhang, Y. A., Ding, X., Wang, X. M., Zhou, Y. N., Zou, L. L., Zellmer, G.
 118 F., and Engling, G.: Carbonaceous aerosol emitted from biofuel household stove combustion in
 119 South China, *Atmosphere*, 11, 112, <https://doi.org/10.3390/atmos11010112>, 2020.

120 Schauer, J. J., Kleeman, M. J., Cass, G. R., and Simoneit, B. R. T.: Measurement of emissions from
 121 air pollution sources. 3. $\text{C}_1\text{-C}_{29}$ organic compounds from fireplace combustion of wood, *Environ. Sci.*
 122 *Technol.*, 35, 1716-1728, <https://doi.org/10.1021/es001331e>, 2001.

123 Schmidl, C., Bauer, H., Dattler, A., Hitzenberger, R., Weissenboeck, G., Marr, I. L., and Puxbaum,
 124 H.: Chemical characterisation of particle emissions from burning leaves, *Atmos. Environ.*, 42,
 125 9070-9079, <https://doi.org/10.1016/j.atmosenv.2008.09.010>, 2008a.

126 Schmidl, C., Marr, L. L., Caseiro, A., Kotianová, P., Berner, A., Bauer, H., Kasper-Giebl, A., and
 127 Puxbaum, H.: Chemical characterisation of fine particle emissions from wood stove combustion of
 128 common woods growing in mid-European Alpine regions, *Atmos. Environ.*, 42, 126-141,
 129 <https://doi.org/10.1016/j.atmosenv.2007.09.028>, 2008b.

130 Sun, J., Shen, Z. X., Zhang, Y., Zhang, Q., Lei, Y. L., Huang, Y., Niu, X. Y., Xu, H. M., Cao, J. J.,
 131 Ho, S. S. H., and Li, X. X.: Characterization of $\text{PM}_{2.5}$ source profiles from typical biomass burning
 132 of maize straw, wheat straw, wood branch, and their processed products (briquette and charcoal) in
 133 China, *Atmos. Environ.*, 205, 36-45, <https://doi.org/10.1016/j.atmosenv.2019.02.038>, 2019.

134 Wang, Z., Bi, X., Sheng, G., and Fu, J.: Characterization of organic compounds and molecular
 135 tracers from biomass burning smoke in South China I: Broad-leaf trees and shrubs, *Atmos. Environ.*,
 136 43, 3096-3102, <https://doi.org/10.1016/j.atmosenv.2009.03.012>, 2009.

137 Yan, C., Zheng, M., Sullivan, A. P., Shen, G., Chen, Y., Wang, S., Zhao, B., Cai, S., Desyaterik, Y.,
 138 Li, X., Zhou, T., Gustafsson, Ö., and Collett, Jr. J. L.: Residential coal combustion as a source of
 139 levoglucosan in China, *Environ. Sci. Technol.*, 52, 1665-1674,
 140 <https://doi.org/10.1021/acs.est.7b05858>, 2018.

141 Zhang, X., Lu, Y., Wang, Q. G., and Qian, X.: A high-resolution inventory of air pollutant
 142 emissions from crop residue burning in China, *Atmos. Environ.*, 213, 207-214,
 143 <https://doi.org/10.1016/j.atmosenv.2019.06.009>, 2019.

144 Zhang, Y.-X., Shao, M., Zhang, Y.-H., Zeng, L.-M., He, L.-Y., Zhu, B., Wei, Y.-J., and Zhu, X.-L.:
 145 Source profiles of particulate organic matters emitted from cereal straw burnings, *J. Environ. Sci.*,
 146 19, 167-175, [https://doi.org/10.1016/S1001-0742\(07\)60027-8](https://doi.org/10.1016/S1001-0742(07)60027-8), 2007.

147 Zhou, Y., Xing, X., Lang, J., Chen, D., Cheng, S., Wei, L., Wei, X., and Liu, C.: A comprehensive
 148 biomass burning emission inventory with high spatial and temporal resolution in China, *Atmos.*
 149 *Chem. Phys.*, 17, 2839-2864, <https://doi.org/10.5194/acp-17-2839-2017>, 2017.

150 **Table S1.** Average concentrations of PM_{2.5}, EC, OC, fossil and non-fossil fractions of EC and OC
151 on ¹⁴C sampling period.

	Winter				Summer	
	IAP haze (n=5)	IAP non- haze (n=2)	PG haze (n=5)	PG non- haze (n=2)	IAP (n=6)	PG (n=5)
	11/24, 11/26, 12/02, 12/03, 12/04	11/22, 12/01	11/24, 11/26, 12/02, 12/03, 12/04	11/22, 12/01	5/24, 5/26, 5/27, 6/10, 6/16, 6/17	5/26, 5/27, 6/10, 6/16, 6/17
PM _{2.5} (μg m ⁻³)	158.7±62.1	30.1±27.3	212.1±84.9	28.9±17.1	42.5±26.5	42.7±21.2
EC (μg m ⁻³)	4.8±1.3	1.2±1.4	6.7±1.6	2.0±0.5	1.1±0.3	2.0±0.7
f _{NF, EC}	0.32±0.03	0.45±0.07	0.39±0.07	0.52±0.00	0.46±0.09	0.41±0.10
OC (μg m ⁻³)	33.8±8.6	9.4±7.4	62.0±19.4	16.4±6.1	8.3±3.2	11.5±4.9
f _{NF, OC}	0.32±0.05	0.32±0.03	0.40±0.07	0.42±0.02	0.46±0.12	0.50±0.09

152 f_{NF, EC} and f_{NF, OC} are the non-fossil fractions of EC and OC.

153

Table S2. Summary of fire spot intensity, transport direction and sources of biomass burning.

Site	Date	PM _{2.5} μg m ⁻³	EC _{nf} μg m ⁻³	LG ng m ⁻³	Fire spots intensity	Transport	Sources of biomass burning
IAP	2016/11/22	10.9	0.14	96.1	Low	from IM and HB	Low intensity
IAP	2016/11/24	117.1	1.35	458.7	Low	from IM and HB	Local
IAP	2016/11/26	209.4	1.43	227.4	High	from IM and HB	Regional
IAP	2016/12/1	49.4	0.82	192.3	High	from IM and HB	Regional
IAP	2016/12/2	98.6	1.51	515.4	High	from IM and HB	Regional + local
IAP	2016/12/3	239.9	1.94	634.8	Low	from HB and SX	local
IAP	2016/12/4	128.6	1.02	321.7	Low	from IM and HB	local
PG	2016/11/22	16.8	0.85	216.6	Low	from IM and HB	Local
PG	2016/11/24	106.8	2.52	915.6	Low	from IM and HB	Local
PG	2016/11/26	239.6	4.34	913.7	High	from IM and HB	Regional + local
PG	2016/12/1	41.0	1.22	311.2	High	from IM and HB	Regional
PG	2016/12/2	138.2	1.34	780.0	High	from IM and HB	Regional + local
PG	2016/12/3	281.5	2.62	1406.3	Low	from HB and SX	Strong local
PG	2016/12/4	294.3	2.70	1796.1	Low	from IM and HB	Strong local
IAP	2017/5/24	12.2	0.55	13.0	High	from IM, LN, HB	Regional
IAP	2017/5/26	34.7	0.44	22.1	High	from IM, HB	Regional
IAP	2017/5/27	78.8	0.49	20.1	High	from IM, HB	Regional
IAP	2017/6/10	18.6	0.46	11.6	Low	from IM, LN, HB	Low intensity
IAP	2017/6/16	44.3	0.40	51.9	High	from SD, HB	Regional + local
IAP	2017/6/17	66.7	0.77	179.6	High	from SX, HB	Regional + local
PG	2017/5/26	37.4	0.58	56.4	High	from SD, HB	Regional
PG	2017/5/27	70.3	0.85	89.8	High	from IM, HB	Regional + local
PG	2017/6/10	11.6	0.65	56.9	Low	from HB, TJ	Local
PG	2017/6/16	47.4	0.72	107.1	Very high	from HB	Regional + local
PG	2017/6/17	46.7	0.96	219.8	Very high	from IM, SX, HB	Regional + local

IM: Inner Mongolia, HB: Hebei, SD: Shandong, SX: Shanxi, TJ: Tianjin

157 **Table S3.** Summary of EC/OC and OC/LG ratios of different biomass types and the ranges of
158 fractions in LG.

No.	Sample	EC/OC	OC/LG	Reference
1	Slash pine	0.141	0.341	Fine et al., 2002
2	Ponderosa pine	0.014	7.83	Fine et al., 2001
3	Western hemlock	0.050	2.52	Hays et al., 2002
4	Loblolly pine	0.178	1.02	Fine et al., 2002
5	Douglas fir	0.098	2.45	Fine et al., 2004
6	Eastern hemlock	0.053	10.5	Fine et al., 2001
7	White pine needle	0.078	7.18	Mazzoleni et al., 2007
8	Larch	0.176	3.68	Schmidl et al., 2008b
9	Balsam fir	0.066	12.3	Fine et al., 2001
10	Douglas fir (catalyst)	0.338	2.52	Fine et al., 2004
11	Loblolly pine	0.307	3.95	Fine et al., 2004
12	Chestnut oak	0.312	3.94	Wang et al., 2009
13	White pine needle	0.282	4.71	Mazzoleni et al., 2007
14	White pine needle	0.242	6.61	Mazzoleni et al., 2007
15	Spruce	0.384	5.02	Schmidl et al., 2008b
16	Mixed wood	0.288	6.76	Mazzoleni et al., 2007
17	White pine needle	0.331	6.64	Mazzoleni et al., 2007
18	Chinese evergreen Chinkapin	0.078	33.8	Wang et al., 2009
19	Chinese red pine	0.375	8.33	Sang-Arlt et al., 2020
20	Cape jasmine	0.137	27.9	Wang et al., 2009
21	Ponderosa pine needles	0.401	10.2	Mazzoleni et al., 2007
22	Common aporosa	0.095	43.3	Wang et al., 2009
23	Samak	0.054	137	Wang et al., 2009
24	Cedar wood	0.090	96.9	Mazzoleni et al., 2007
25	Excelsior	1.080	5.87	Mazzoleni et al., 2007
26	Excelsior	1.090	6.13	Mazzoleni et al., 2007
27	Eastern white pine	0.426	19.1	Fine et al., 2001
28	Maritime pine	1.420	6.87	Goncalves et al., 2010
29	China fir	0.651	16.7	Sang-Arlt et al., 2020
30	Ponderosa pine needles	1.320	15.4	Mazzoleni et al., 2007
31	Cedar wood	0.264	94.4	Mazzoleni et al., 2007
32	Ponderosa pine needles	1.500	17.4	Mazzoleni et al., 2007
33	Wood	0.500	55.6	Schmidl et al., 2008a
34	Ponderosa pine needles	0.632	55.4	Mazzoleni et al., 2007
35	Tamarak pine wood	0.330	137	Mazzoleni et al., 2007
36	Ponderosa pine sticks	3.320	20.1	Mazzoleni et al., 2007
37	Ponderosa pine sticks	3.680	25.6	Mazzoleni et al., 2007
38	Wood branch charcoal	0.393	625	Sun et al., 2019
39	Spruce with green needles	0.401	2128	Schmidl et al., 2008b

40	Pine	0.508	2128	Schauer et al., 2001
41	Pine with green needles	0.600	3571	Schauer et al., 2001
No.	Sample	EC/OC	OC/LG	Reference
42	Wheat straw	0.223	4.07	Sun et al., 2019
43	Wheat straw	0.068	15.4	Fushimi et al., 2017
44	Wheat straw	0.083	15.2	Fushimi et al., 2017
45	Wheat straw	0.184	12.5	Dhammapala et al., 2007
46	Wheat straw	0.422	10	Hays et al., 2005
47	Wheat straw	0.510	9.09	Mazzoleni et al., 2007
48	Maize straw	0.257	3.18	Sun et al., 2019
49	Maize straw	0.106	55.6	Yan et al., 2018
50	Cereal straw	0.130	12	Zhang et al., 2007

160 **Table S4.** The estimated $OC/EC_{nf, min}$ and $OC/EC_{f, min}$ ratios for IAP and PG sites during the whole
161 winter and summer sampling period

	lowest 5 % OC/EC	lowest 2 $\frac{f_{NF,OC}}{f_{NF,EC}}$	lowest 2 $\left(\frac{1-f_{NF,OC}}{1-f_{NF,EC}}\right)$	Estimated $OC/EC_{nf, min}$	Estimated $OC/EC_{f, min}$
IAP winter	4.35	0.70	0.96	3.06	4.16
PG winter	6.27	0.76	0.81	4.76	5.09
IAP summer	4.65	0.73	0.78	3.41	3.62
PG summer	4.45	0.88	0.62	3.92	2.76

162 $f_{NF, OC}$ and $f_{NF, EC}$ are the non-fossil fractions of OC and EC, $(1 - f_{NF, OC})$ and $(1 - f_{NF, EC})$ are the fossil
163 fractions of OC and EC.
164

165 **Table S5.** Correlations and slopes among WINSOC, WSOC, POC, SOC, OC_{bb} and OC_{ck} at IAP
166 and PG in winter and summer.

x	y	IAP winter		PG winter		IAP summer		PG summer	
		slope	R ²	slope	R ²	slope	R ²	slope	R ²
POC _f	WINSOC _f	1.11	0.97	1.23	0.97	0.92	0.93	0.84	0.82
	WSOC _f	0.57	0.99	0.61	0.84	0.96	0.92	0.58	0.55
SOC _f	WINSOC _f	1.53	0.96	1.27	0.89	0.99	0.91	0.98	0.45
	WSOC _f	0.78	0.93	0.69	0.96	1.05	0.93	0.89	0.67
OC _{bb}	WINSOC _{nf}	1.59	1.00	2.38	0.94	1.16	0.44	1.58	0.91
	WSOC _{nf}	1.64	0.94	1.70	0.92	3.41	0.93	1.54	0.93
OC _{ck}	WINSOC _{nf}	3.54	0.88	1.68	0.69	1.08	0.74	2.26	0.27
	WSOC _{nf}	3.83	0.94	1.21	0.69	1.53	0.19	2.29	0.32
SOC _{nf}	WINSOC _{nf}	0.85	0.98	0.98	0.83	0.42	0.65	0.79	0.92
	WSOC _{nf}	0.90	0.99	0.71	0.83	1.09	0.97	0.75	0.88

167 f: fossil sources, nf: non-fossil sources, bb: biomass burning, ck: cooking. Concentrations of fossil
168 and non-fossil sources of WINSOC and WSOC were from ¹⁴C measurement. POC, SOC, OC_{bb} and
169 OC_{ck} are from extended Gelencsér method.

170

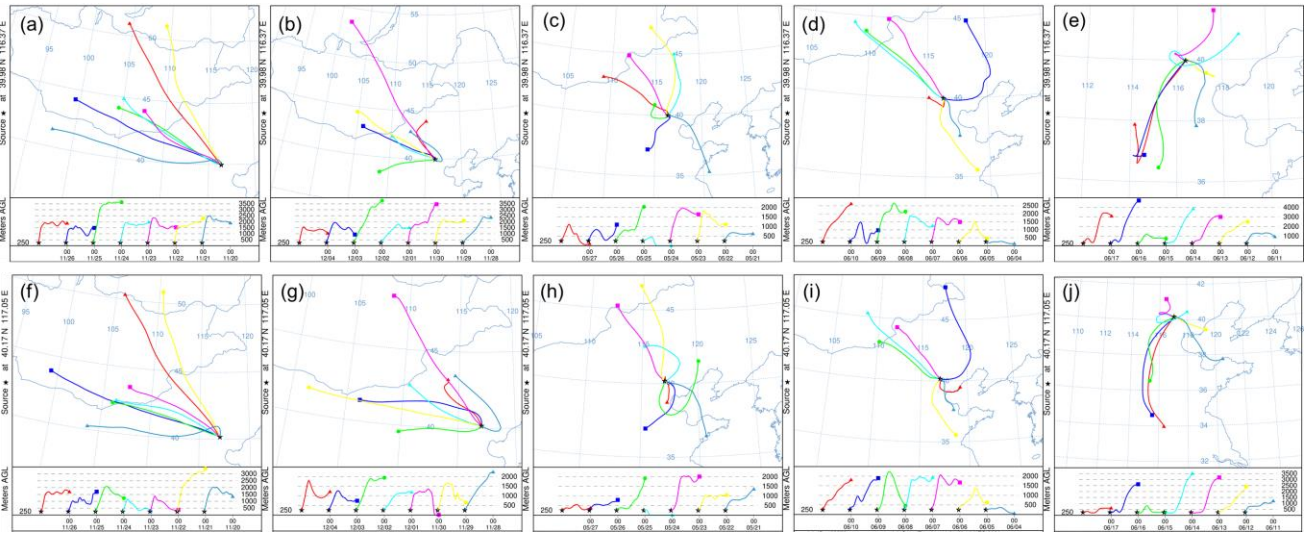


Figure S1. 48 h air-mass back trajectories with 24 h interval at 250 m, (a)-(e): destination at IAP, (f)-(j): destination at PG. (<https://ready.arl.noaa.gov/HYSPLIT.php>, last access: 12 June 2020)

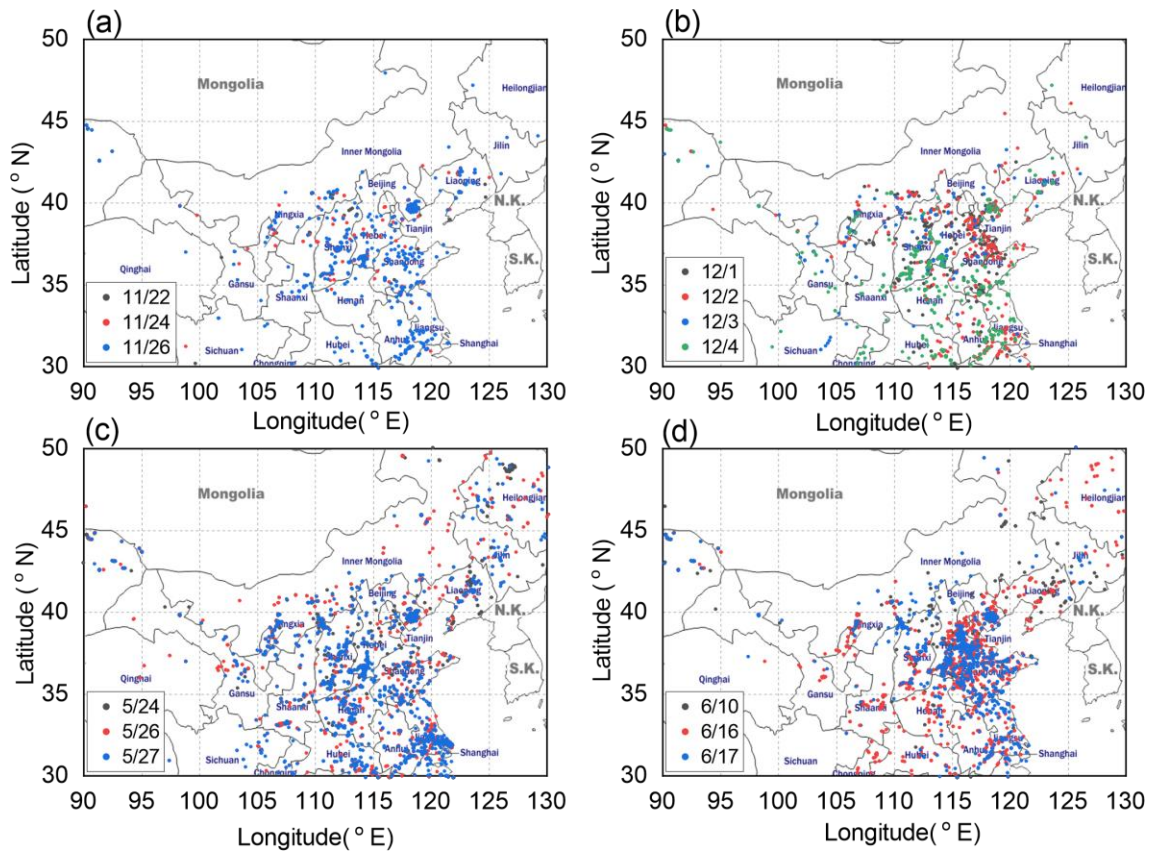


Figure S2. Fire spots observed by MODIS (AQUA/TERRA) (<https://firms.modaps.eosdis.nasa.gov/alerts/>, last access: 16 April 2020) around Beijing, coloured dots refer to fire spots on (a): 22, 24, 26 Nov 2016, (b): 1-4 Dec 2016, (c): 24, 26, 27 May 2017, (d) 10, 16, 17 Jun 2017.

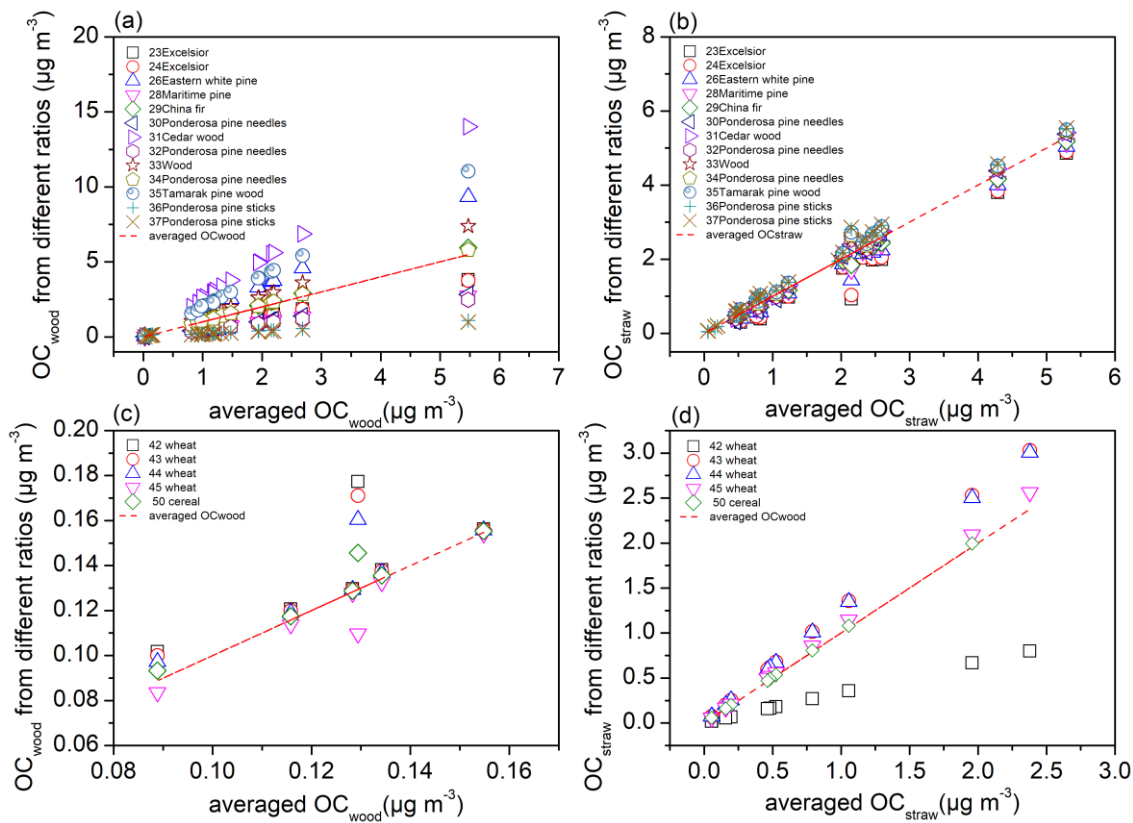


Figure S3. Correlations of averaged OC_{wood} with OC_{wood} from different ratios and averaged OC_{straw} with OC_{straw} from different ratios. (a), the influence of ratios from softwood on the estimation of OC_{wood} ; (b), the influence of ratios from softwood on the estimation of OC_{straw} ; (c), the influence of ratios from wheat straws on the estimation of OC_{wood} ; (d), the influence of ratios from wheat straws on the estimation of OC_{straw} . As there is only one set of ratios from maize straw which matches the selection limitation, the influence of ratios from maize straw was not plotted. The legends correspond to the No. and types of samples in Table S3.

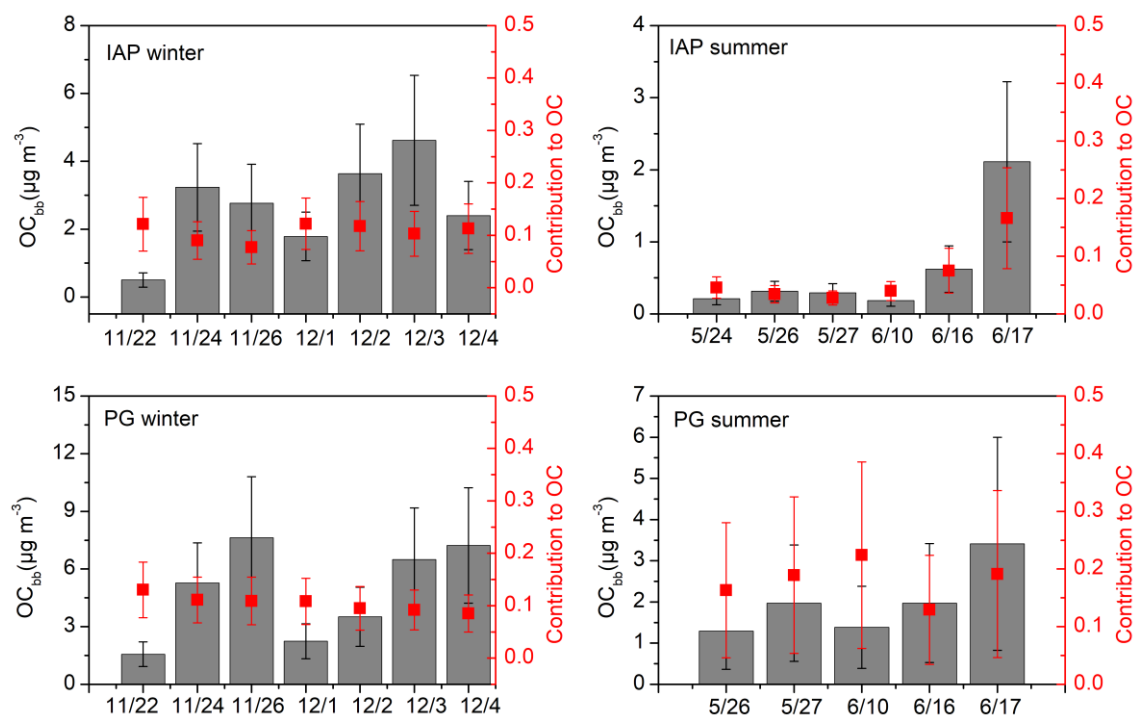


Figure S4. The mass concentrations and % contributions of OC_{bb} at IAP and PG during winter and summer.

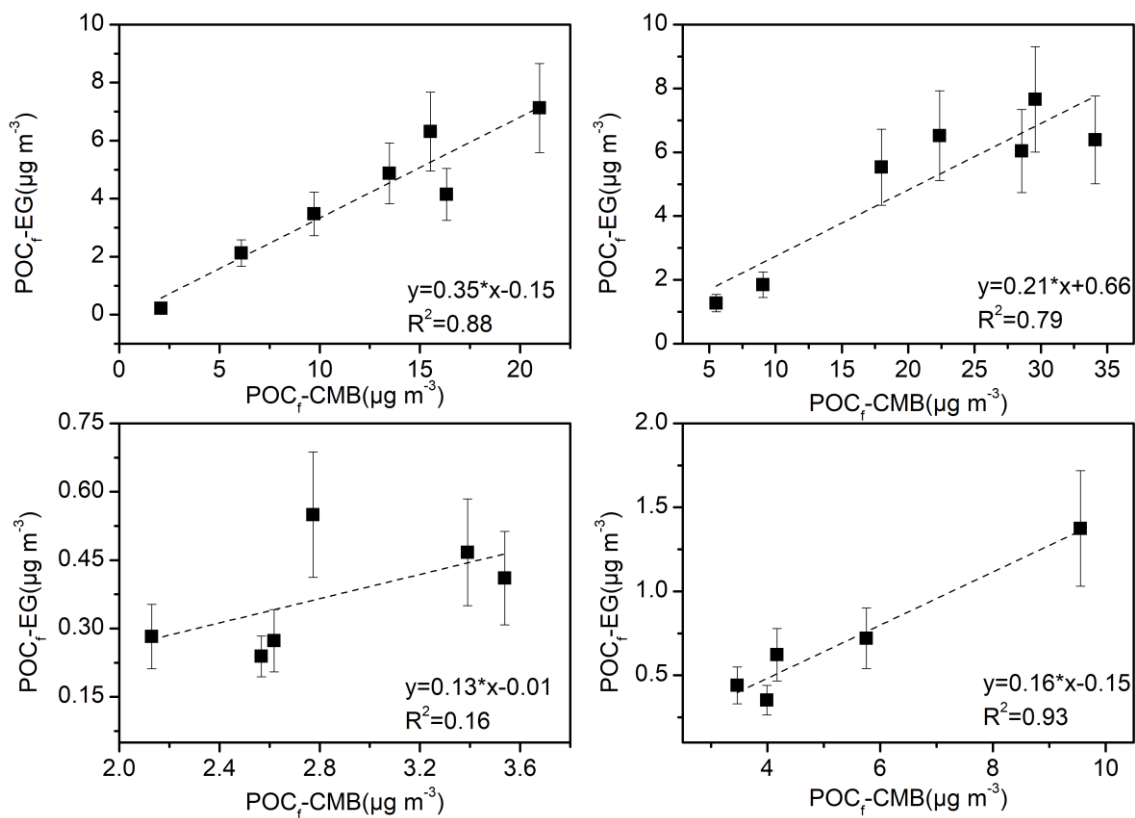


Figure S5. Correlations of POC_f from the extended Gelencsér method ($\text{POC}_f\text{-EG}$) and CMB if using $(\text{POC}/\text{EC})_f$ ratios 1.12–2.08 in winter, 0.40–0.77 in summer.

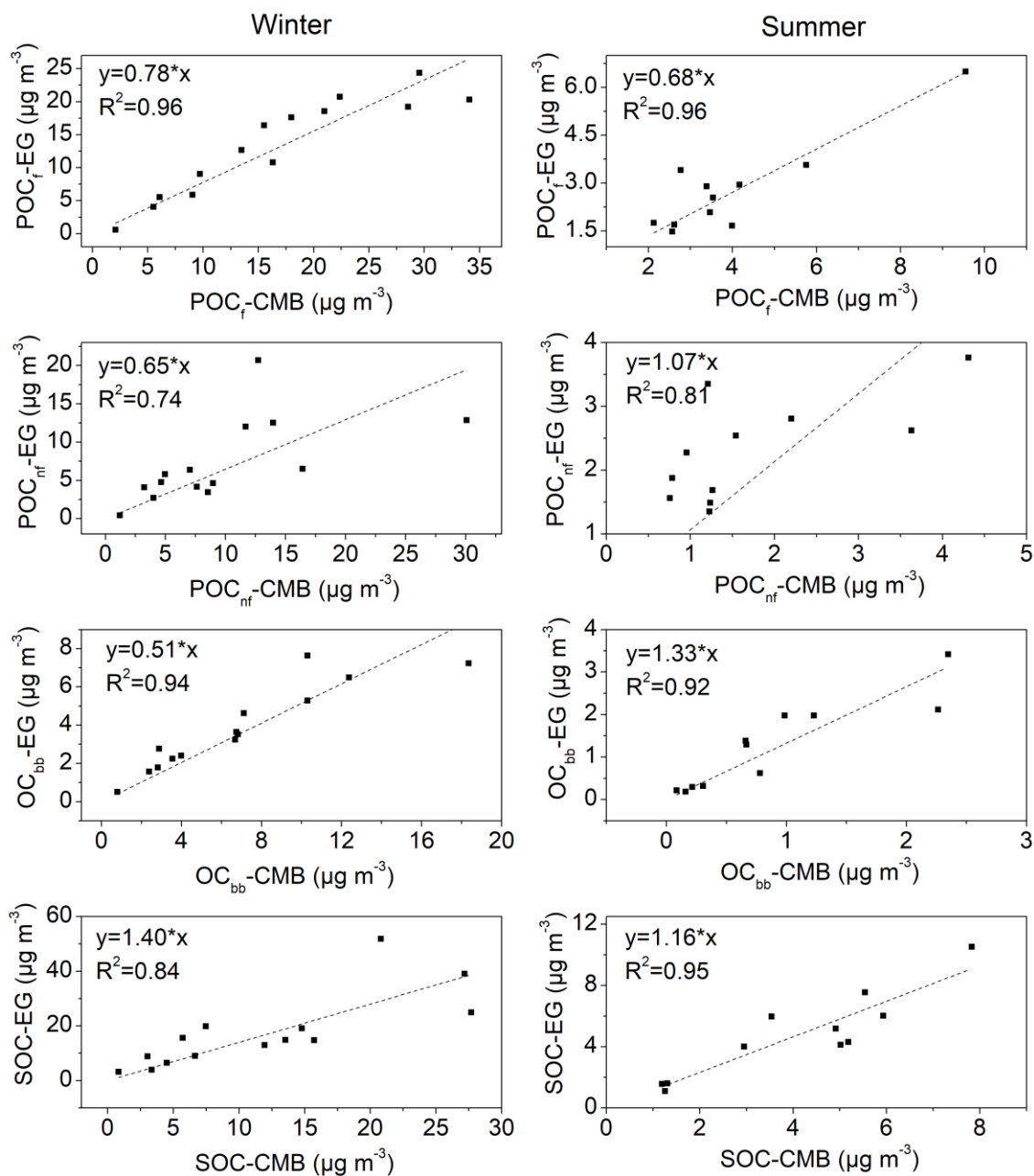


Figure S6. Correlations of OC sources from extended Gelencsér method with those from CMB model in winter (left) and summer (right). EG denotes extended Gelencsér method.

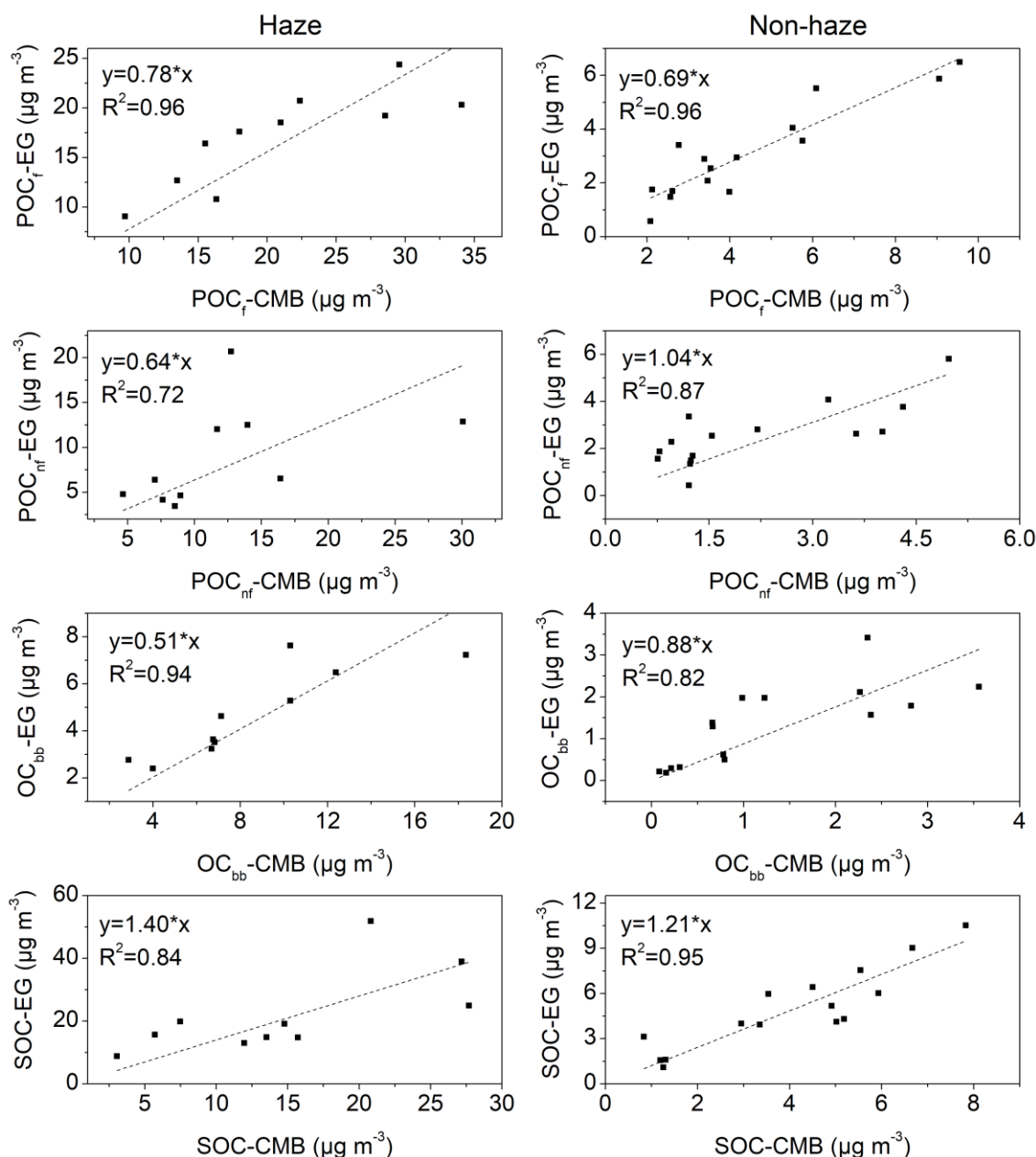


Figure S7. Correlations of OC sources from extended Gelencsér method with those from CMB model during haze period (left) and non-haze period (right). EG denotes extended Gelencsér method.